Molybdenum drawdown during Cretaceous Oceanic Anoxic Event 2

Tatiana Goldberg[1,5*], Simon W. Poulton[2], Thomas Wagner[3], Sadat F. Kolonic[4], Mark Rehkämper[1]

[1]Department of Earth Science and Engineering, Imperial College London, London, SW7 2AZ, UK

[2]School of Earth and Environment, University of Leeds, Leeds, LS2 9JT, UK

[3]School of Civil Engineering and Geosciences, Newcastle University, Drummond Building, Newcastle upon Tyne, NE1 7RU, UK

[4]Shell Petroleum Development Company of Nigeria, Reservoir and Production Geochemistry, Port Harcourt, Nigeria.

[5]TNO, Department of Geo-Energy, Utrecht, 3584 CB, The Netherlands

***** corresponding author: tanya.goldberg@tno.nl

Keywords: Molybdenum isotopes, δ^{98}Mo, OAE2, Cretaceous, proto-North Atlantic

Abstract

During the Cretaceous greenhouse, episodes of widespread ocean deoxygenation were associated with globally occurring events of black shale deposition. Possibly the most pronounced of these oceanic anoxic events (OAE's) was the Cenomanian-Turonian OAE2 (~94 Ma). However, although certain redox sensitive trace metals tend to be preferentially sequestered in sediments deposited under anoxic conditions, with Mo drawdown being specifically prone to euxinic settings, these elements are generally somewhat depleted in sediments deposited during OAE2. To understand the driving factors responsible for this depleted trace metal drawdown, we have studied a low latitude section from the proto-North Atlantic Ocean (Tarfaya S57), where existing biomarker and iron-sulphur data point to a dominantly euxinic water column, with periodic transitions to ferruginous (Fe-rich) water column conditions. We utilise a variety of redox proxies (Fe-speciation, redox sensitive trace metals and Mo isotopes), which, in combination, allows us to evaluate the detailed nature of ocean redox conditions and hence controls on trace metal drawdown. The results suggest that seawater δ^{98}Mo values may have ranged between ~ 0.6 and 1.1‰ during OAE2, likely connected to changes in the local Mo reservoir as a consequence of low and probably heterogeneous concentrations of Mo in the ocean. The very low Mo/TOC ratios at Tarfaya and elsewhere in the proto-North Atlantic may support a model in which deep-water circulation was partially restricted within and between the North Atlantic and other ocean basins. We propose that the combination of a low and possibly heterogeneous δ^{98}Mo of seawater Mo, together with low Mo/TOC ratios, points to a large decrease in the global oceanic Mo reservoir during OAE2, reflecting a major global scale increase in Mo drawdown under persistent euxinic conditions.

1. Introduction

The Cretaceous was a time of high global temperatures as a consequence of elevated atmospheric CO_2[1]. A series of major black shale deposition events during intervals of ocean deoxygenation (termed oceanic anoxic events; OAEs) were associated with these extreme greenhouse conditions[2]. These fluctuations in Cretaceous seawater redox conditions coincided with massive perturbations to the carbon and nutrient cycles within and between the main global reservoirs[1]. During the Cenomanian-Turonian (Bonarelli) event (OAE2) at ~95 Ma, a worldwide positive carbon isotope excursion documents the globally enhanced burial of marine organic carbon under anoxic conditions[2], likely driven by a global-scale increase in primary productivity[3-5].

Anoxic conditions favoured the widespread deposition of organic-rich black shales during and intermittently prior to OAE2, in the proto-North Atlantic and western Tethys Ocean[6-9] and in other regions[10]. Several studies have argued that sluggish circulation within the proto-North Atlantic and restricted deep-water exchange with other ocean basins[1,7] was responsible for black shale deposition[11,12]. However, other studies have postulated that sufficient ocean circulation existed to allow rigorous water exchange with the surrounding ocean basins[13].

Under anoxic conditions, many redox sensitive trace metals are preferentially deposited[14,15], with Mo drawdown being specifically prone to euxinic (free H_2S) settings[16]. However, during the onset of OAE2 a severe depletion of sedimentary Mo, V, Zn, Cr, Ni and U (relative to total organic carbon; TOC) has been reported for the North Atlantic[8,9]. This observation has been explained by a reduction in the marine trace element inventory due to the enhanced drawdown of redox sensitive elements through expansion of euxinic waters[9]. However, low Mo/TOC ratios in euxinic sediments have also been suggested to be typical of silled marine basins, where resupply of Mo via deep water renewal was limited, resulting in lower oceanic Mo concentrations and hence less uptake of Mo per unit of organic matter compared to fully connected ocean basins[17,18]. This raises the question as to whether

drawdown of Mo during OAE2 occurred on a local, regional or global scale, with consequences for identifying the global extent and severity of ocean anoxia during a period of massive, global carbon-climate perturbation.

Mo isotopes have emerged as a powerful tool for evaluating the global extent of ocean euxinia and the size of the oceanic Mo repository[19-22]. The relative extent of oxic and anoxic sinks defines the amount and isotopic composition of Mo remaining in seawater (see supplementary information). The ability of Mo isotopes to capture the seawater signal is, however, limited to highly sulfidic environments, whereas under both oxic conditions and anoxic conditions where H_2S is absent or concentrations are low, a wide range of Mo isotope signatures may be encountered (Fig. 1).

This study focuses on a low latitude W-African shelf setting of the proto-North Atlantic Ocean (Tarfaya Basin). We present high resolution (~0.3 ka scale) Mo isotope data that cover the initial onset and first part of the maximum perturbation of OAE2, as defined by the positive carbon isotope excursion[8,23]. To determine the fidelity of sedimentary Mo isotopes to reflect seawater values, we critically appraise the Mo isotope composition of marine sediments with new and existing data that document local redox conditions (Fe-speciation, organic carbon contents, biomarkers and trace elements). Indeed, while the sediments were predominantly deposited under sulfidic conditions[8,24], regular cyclic (orbital timescale) transitions to anoxic, Fe-rich (ferruginous) water column conditions were also a prominent feature[25]. By combining hydrographic and geochemical aspects, our Mo isotope data provide a new view on euxinic water mass expansion and extensive Mo drawdown during OAE2.

1.1 The Late-Cretaceous Tarfaya shelf basin

The Tarfaya Basin is located on the northwestern margin of the Sahara Craton. During the Late-Cretaceous, the basin was situated at a latitude of ~15° N in a marine shelf setting open to the proto-North Atlantic Ocean (Fig. 2)[7,8,12,24,26]. The N-African palaeo-coast is proposed to have been in the centre of an upwelling zone that covered large parts of the

subtropical African margin and was responsible for providing nutrient-rich water and fostering the establishment of anoxia/euxinia[7,8,12,24].

Core samples were obtained from drill site S57 of the Tarfaya Basin, covering the core interval between 50.04 to 54.35 m. Palaeowater depths at site S57 have been estimated as ~250 to 300 m[8]. The section consists of pelagic organic-rich carbonates and marls, with 2 to 20 wt.% TOC and very little terrigenous input[8]. Turbidites are absent from the studied part of the section. The last occurrence of *Rotalipora cushmani* (~93.9 Ma) was found at ~51.2 m[23]. The studied section covers the upper $\delta^{13}C$ phase A to lower phase B with a positive $\delta^{13}C$ excursion from -27 to -23‰ (Fig 3)[8]. Spectral analyses, based largely on cyclicity in organic matter content, point to a dominance of obliquity forcing with a calculated average sedimentation rate for the covered interval of ~6 cm/ka[27].

2. Methods

For trace element and Mo isotope analyses, 50 to 100 mg of sample powder was digested in a mixture of HF (Optima, Fisher Scientific), HNO_3 (purified by sub-boiling distillation in quartz stills) and $HClO_4$ (Omnipure, Fisher Scientific). The total Mo blank for this procedure was ~0.12 ng. Once dissolved, an aliquot of the sample solution was analysed for trace elements with a Varian ICP-MS instrument (Natural History Museum London). The remaining solution was spiked with a Mo double-spike (to a 1:1 sample/spike ratio) for subsequent stable isotope analyses. The chromatographic purification of Mo is described in Goldberg et al. (2013)[28]. All isotopic measurements were performed with a Nu Instruments MC-ICP-MS (Department of Earth Science and Engineering, Imperial College London). For further method specifications see Goldberg et al. (2013)[28]. The samples were initially measured relative to the in-house ICL-Mo isotope standard and these results were subsequently re-normalised to NIST SRM 3134[28]. Replicate analyses of several samples show a typical reproducibility of better than ± 0.1‰ (2sd). The uncertainties (2sd) for the element concentration measurements are better than ± 5% for Mo, Cr, U, Cd, Zn, and Re (at >0.1 ppb)

and better than ± 10% for Re contents of <0.05 ppb. The Fe-speciation and total organic carbon contents (TOC) are from Poulton et al. (2015)[25], organic carbon $\delta^{13}C$ values are from Tsikos et al. (2004)[23], and additional trace metal data are from Kolonic et al. (2005)[8].

3. Results and Discussion

3.1 Evaluation of local redox conditions

The sediments contain high but variable concentrations of TOC (Fig. 3), from 2 to 20%[8,25,29]. Most of the TOC-rich sediment is laminated with no visible bioturbation, implying anoxic deposition. Between 51.74 and 53.06 m, however, intermittent bioturbation is evident, with greatest intensity between 51.89 and 52.00 m, spanning roughly 2 ka. This provides evidence for short-lived intervals of dysoxic-oxic conditions, which allowed larger benthic fauna to infiltrate the sediment. Notably, these oxic intervals are not recorded by fluctuations in the relative proportions of carbonate and organic carbon, and are thus not easily detected by bulk geochemical data (which integrates longer time periods). It is difficult to estimate the actual duration of these oxygenated periods because even short-lived water column oxygenation can result in bioturbation to several centimetres depth.

The Fe speciation proxy is based on the presence or absence of enrichments in (bio)geochemically available Fe minerals, termed highly reactive Fe (FeHR). Ratios of highly reactive Fe to total Fe (FeHR/FeT) that exceed 0.38 provide evidence for anoxic depositional conditions[30]. Providing FeHR/FeT exceeds 0.38, the extent of pyritization of the highly reactive Fe pool (FeP/FeHR >0.7 to 0.8) defines whether the bottom water was anoxic and ferruginous (Fe-rich) or euxinic (containing H_2S). Throughout our analysed section, Fe-speciation points to persistent anoxic bottom water conditions, with FeHR/FeT > 0.38 (Fig. 3)[25]. Short-lived oxic intervals are not resolved at our sampling resolution. According to the most recent dating constraints[8,27], our analyses of Fe-speciation for 2 cm intervals of sediment have an average resolution of ~0.3 ka. Nevertheless, the absence of bioturbated intervals throughout most of the section suggests that such episodes were not common or, if

so, of very short duration. More detailed consideration of the extent of sulfidation of the FeHR pool (FeP/FeHR) suggests that bottom waters at S57 in the Tarfaya Basin fluctuated between ferruginous (FeP/FeHR <0.7) and euxinic (Fig. 3)[25], while the presence of isorenieratane in euxinic intervals suggests that sulfide extended from bottom waters into the lower photic zone[8,25].

The preferential deposition of redox sensitive trace elements (e.g. Mo, U, V, Re, Cr) to the sediment under anoxic to euxinic conditions has led to their exploitation as local redox indicators (see supplement). Throughout the studied section, enrichment factors (EF) for Mo (EF = 11 to 415, average 89), V (EF = 3 to 59, average 12) and U (EF = 11 to 201, average 36) suggest significant drawdown of these elements relative to "Post-Archean Average Shale" (Fig. 4; Table S1), consistent with deposition within an anoxic water column[31,32]. However, the enrichment factors do not vary systematically between periods of ferruginous and sulfidic conditions, which in particular might be expected for sulfide-sensitive Mo (Figs. 3 and 4). Rather, the EF variation is primarily connected to the abundance of organic matter[17], as demonstrated by a correlation between Mo, U, V and TOC (Fig. 5). However, Poulton et al. (2015)[25] suggest that very short-lived episodes of water column euxinia occurred during the ferruginous intervals (as suggested by periodically high Fe_{py}/Fe_{HR} ratios and the low-level presence of biomarkers indicative of photic zone euxinia), with dissolved sulfide being persistently present in the sediment pore waters. Euxinic episodes within the dominantly ferruginous intervals would provide an explanation for persistent Mo drawdown during these intervals, although such enrichments could also have been a consequence of sulfidic porewaters near-the sediment-water interface, allowing Mo diffusion and sequestration from the overlying water column.

Rhenium and Cr are also enriched above the crustal background (Fig. 4, Table S1) throughout the section, as a result of anoxic sequestration. In comparison to Mo, however, Re is more efficiently deposited under dysoxic to anoxic, non-sulfidic conditions[14,33]. This has led to the use of Re/Mo ratios to constrain changes in the local redox environment[34], specifically

159 to differentiate between sulfidic and low-oxygen, non-sulfidic conditions[14,19,20]. Similar
160 observations have been made with regard to Cr, which may undergo dissolution under
161 sulfidic conditions, possibly due to breakdown of organically bound Cr species[15]. Thus,
162 variability in Re/Mo and Cr/Mo ratios throughout the anoxic water column at S57 likely
163 documents variations in dissolved sulfide availability, which is important for evaluating the
164 Mo isotope signal. The Re/Mo and Cr/Mo ratios (Fig. 4) are high (mostly ≥0.02 and ≥0.10,
165 respectively) across the middle ferruginous intervals (F2 and F3) and during the second and
166 third euxinic intervals (E2 and E3), indicating weakly euxinic conditions with limited Mo
167 sequestration. For the remaining part of the section, Re/Mo and Cr/Mo are low (<0.1 and
168 <10, respectively), consistent with enhanced Mo drawdown under elevated concentrations of
169 dissolved sulfide.
170
171 ***3.2 Hydrography and Mo reservoir***
172 A conspicuous feature of the investigated section is the low sedimentary Mo/TOC
173 values, ranging from 0.2 to 2.4×10^{-4}, with an average of 1×10^{-4} (Figs. 5A, 6), despite euxinic
174 bottom water conditions throughout much of the succession. Today, low bottom water Mo
175 concentrations tend to be recorded in semi-isolated sulfidic basins, such as the Black Sea,
176 where higher rates of Mo burial than Mo resupply and long deep water residence times
177 (>500 years) result in low Mo/TOC ratios of $4.5 \pm 1\times10^{-4}$ [17]. In contrast, weakly restricted
178 anoxic basins, such as the Saanich Inlet (SE of Vancouver Island, Canada) have shorter deep
179 water residence times (<2 years) and Mo/TOC ratios of $\sim45 \pm 5\times10^{-4}$ [17]. Low sedimentary
180 Mo/TOC ratios also occur in oxic and suboxic bottom waters, where the redoxcline is below
181 the sediment-water interface. For example, in open marine upwelling systems, such as the
182 modern Namibian shelf, rapid water mass exchange prevents sufficient build-up of H_2S and
183 lower Mo/TOC ratios of $\sim6 \pm 3\times10^{-4}$ are recorded[17]. The low Mo/TOC values at Tarfaya S57,
184 however, cannot be a result of insufficient H_2S build-up as in the example of the modern

185 Namibian shelf, because predominantly sulfidic and periodically anoxic ferruginous bottom
186 water conditions are supported by Fe-speciation, high TOC, S-isotopes and the abundance of
187 isorenieratane[25].

188 Alternatively, the low Mo/TOC ratios recorded at Tarfaya may have been a
189 consequence of severe restriction of basin-wide ocean circulation. Algeo and Tribovillard
190 (2009)[31] proposed that specific trends in sedimentary Mo and U EFs can be compared to the
191 Mo/U ratio of modern seawater to estimate the degree of basinal restriction (see Fig. 7). For
192 the Tarfaya section, the Mo and U EFs are predominantly high and they coincide with the
193 open marine trend, with relatively few values falling towards the basinal restriction line (Fig.
194 7), thus negating severe restriction as a likely explanation for low Mo/TOC.

195 With the onset of OAE2, a distinct decline in Mo/TOC ratios is evident in the Tarfaya
196 section, from ~4 to ~1×10^{-4} (Fig. 6). Despite evidence for anoxia on the Tarfaya shelf prior to
197 the global expression of OAE2[25], it is unlikely that anoxic bottom water conditions were more
198 globally prevalent prior to, rather than during, OAE2[4,6,8,9]. Therefore, this Mo/TOC trend is
199 unlikely to be linked to more oxygenated bottom water conditions during OAE2.

200 At Demerara Rise off tropical South America, Hetzel et al. (2009)[9] observed a similar
201 decline in Mo/TOC from ~9×10^{-4} before OAE2 with values dropping to an average of ~2×10^{-4}
202 during OAE2 (Table 1; Fig. 2). At Demerara Rise, Mo (EF = 143 to 163) and U (EF = 17 to 30)
203 enrichments point towards an unrestricted, euxinic water body. Westermann et al. (2014)[22]
204 report a decrease in average Mo/TOC from $11x10^{-4}$ prior to OAE2 to $5\ x10^{-4}$ during OAE2 in
205 anoxic sediments at site 367 (Cape Verde Basin), and low average Mo/TOC of ~$2\ x10^{-4}$ at
206 ODP site 1276 during OAE2 (Fig. 2). The overall low Mo and U EFs at these sites point to an
207 unrestricted water body[22]. Alternating, hemipelagic euxinic OAE2 black claystones from
208 DSPD Site 603 (Fig. 2) in the northern part of the proto-North Atlantic also have Mo/TOC
209 ratios of 2 to 5×10^{-4} (average 2.8)[6]. Circulation patterns and palaeogeographic conditions do
210 not imply isolation of Demerara Rise or the proto-North Atlantic[35], nor do bulk geochemical
211 and molecular patterns[6,12], suggesting that deep water Mo concentrations were low

throughout the Cenomanian/Touronian proto-North Atlantic. In the central proto-North Atlantic (DSDP Site 368; Fig. 2), Mo/TOC values of 5×10^{-4} from anoxic/sulfidic sediments are consistent with low Mo concentrations[36]. A contrasting picture is drawn by Mo/TOC values of ~300 in the run-up, during and after OAE2 at ODP site 641 (Table 1). The origin of such extreme enrichments was attributed to either proximity to hydrothermal vents or to very low sedimentation rates[36], although similar sedimentation rates are associated with much lower Mo/TOC values at other sites[9]. A further process that may lead to high Mo concentrations is the operation of a metal-oxyhydroxide particulate shuttle (Figure 7)[32]. This process has also been inferred for sites 367 and 1276[22]. Fluctuating redox conditions cause Mo to be captured by Mn- (and Fe) oxides, released, and re-captured within the sulphide layer repeatedly, thus accelerating the transfer of Mo to the seafloor[32].

Outside the proto-North Atlantic, stratigraphically equivalent anoxic/euxinic OAE2 sections, the Calabiancia, Bottacione, Contessa and Furlo sections in the western Tethys (Fig. 2), show Mo/TOC averages of 2×10^{-4}, 4×10^{-4}, 3×10^{-4} and 9×10^{-4}, respectively (Table 1)[22,32]. The latter two were however, deposited in anoxic, non-euxinic conditions with possible contribution of Mo from metal-oxyhydroxide particulate shuttling[22]. In the Angola Basin (Site 530, Fig. 2) average Mo/TOC ratios of anoxic shales are somewhat, but not significantly, higher (Table 1)[37]. The oceanographic setting and U-Mo systematics imply that these South Atlantic basins were also open to water exchange with the deep oceans and adjacent basins (Fig. 7)[22,32,37]. In combination, available data suggest that deep water Mo concentrations may have been somewhat higher outside of the proto-North Atlantic, but possibly lower than in weakly restricted euxinic environments of the present (e.g., Saanich Inlet Mo/TOC average = $45\times10^{-4} \pm 5\times10^{-4}$)[17]. During the Cenomanian-Turonian period, deep water exchange with the proto-North Atlantic occurred largely (if not solely) through the Western Tethys and the Central American-Pacific Seaways[7,13,35], although the degree of exchange is still highly debated. The hydrographic restriction of the proto-North Atlantic could thus have led to basin wide Mo depletion during extended euxinic periods. However, unless the Tethys and

South Atlantic were equally restricted, the low Mo/TOC values of the North Atlantic sections point to a more global mechanism of Mo depletion.

3.3 Constraints on δ^{98}Mo to reflect seawater

To assess possible global mechanisms we draw upon Mo isotopes, which can give insight into the spatial extent of euxinic conditions during OAE2. Mo isotopes can only be exploited as a global redox proxy if sedimentary δ^{98}Mo records the global Mo seawater value. The δ^{98}Mo of seawater is thought to be captured in sediments deposited under highly sulfidic (>11 μM H_2S_{aq}) bottom waters, when all Mo exists in the form of MoS_4^{2-} and is quantitatively scavenged to sinking particles[16,38]. Transformation of MoO_4^{2-} to $MoOS_3^{2-}$ via thiomolybdate intermediates is relatively rapid (on a timescale of days), whereas the reaction kinetics for full conversion of $MoOS_3^{2-}$ to MoS_4^{2-} are slow (on a timescale of years) and can only be completed in a water body with prolonged sulfidic conditions[39,40]. Consequently, a semi-restricted basin with a euxinic water column is the ideal setting for tracing seawater Mo[40,41]. The semi-isolated proto-North Atlantic offers such a setting. The palaeo-redox indicators utilised in this study provide evidence for prolonged cyclic intervals of euxinia in the Tarfaya Basin during OAE2, allowing us to specifically target samples that likely best record the seawater δ^{98}Mo signal.

Higher δ^{98}Mo values close to seawater would be expected in highly sulfidic environments, and lower (farther removed from seawater) δ^{98}Mo values are anticipated under ferruginous bottom water conditions[41,42]. The results shown in this study are, however, not in accord with this expectation (Fig. 4). In fact, δ^{98}Mo values do not reveal a specific trend associated with the ferruginous-euxinic redox fluctuations. At the top and bottom of the studied section, δ^{98}Mo remains relatively stable throughout the euxinic and ferruginous intervals, whereas positive and negative δ^{98}Mo shifts occur within euxinic intervals E2 and E3, and ferruginous interval F3 (Fig. 4).

We observe three distinct δ^{98}Mo clusters/trends throughout the studied section:

I. Low δ^{98}Mo values of -0.3 to 0.1‰ between 53.12 and 52.10 m, during period E2.

II. Relatively constant δ^{98}Mo in the lower (F1, E1 and F2) and upper (upper E3, F4 and E4) sections, with an average value of 0.6 ± 0.1‰ (NIST).

III. Intermittent shift to higher δ^{98}Mo of ~ 1.1‰ between 52.1 and 51.5 m, corresponding to F3 and lower E3.

3.3.1 I. Low δ^{98}Mo values of -0.3 to 0.1‰

We propose that the low δ^{98}Mo values do not reflect either global or local seawater, despite having been recorded in a sulfidic interval (according to Fe-speciation). The main reason to negate a seawater origin is that values of -0.3 to 0.1‰ are lower than the modern input value of ~0.4‰[43]. As there is no documented process that exerts positive Mo isotope fractionations, seawater δ^{98}Mo cannot be less than the δ^{98}Mo value of the Mo input to the ocean (Fig. 1). Although the Mo isotope compositions of riverine and hydrothermal inputs to the ocean may have varied in the past[44], the δ^{98}Mo value of the total input should not have been lower than ~0.1‰[21,43,44]. There are, however, several possible reasons for low δ^{98}Mo values.

1. Influence of freshwater input, lowering the local seawater signal

McArthur et al. (2008)[18] suggested that low Mo/TOC (< ~0.5) is indicative of total water mass isolation, where δ^{98}Mo is largely influenced by freshwater input. The cyclic enhancement of reactive iron inputs, driven by increased silicate weathering during humid periods, may explain the cycling between euxinic and ferruginous water column conditions in the Tarfaya Basin[25]. If correct, seawater δ^{98}Mo would have been driven towards lower values during periods of enhanced riverine inputs (Fig. 1) or would have at least fluctuated during ferruginous intervals. In this respect, the lack of covariation between FeP/FeHR and δ^{98}Mo, and the relatively stable δ^{98}Mo signal throughout the upper and lower parts of the section,

argues that δ^{98}Mo of the Tarfaya waters was not strongly affected by variations in fluxes from the continent.

2. Operation of a Mn-Fe-oxyhydroxide shuttle

During short intervals of ferruginous conditions Mo would have been sequestered into Mn-oxyhydroxides, which is connected with an isotope fractionation towards low δ^{98}Mo values (Barling & Anbar, 2004). Upon change to a euxinic water column, Mo would have been released via Mn-oxyhydroxide dissolution and sequestered (quantitatively) as MoS_4, thus retaining the low Mo isotope composition[22,46]. The same process also operated with Fe-(oxyhydr)oxides, although these exert a smaller isotopic fractionation between seawater Mo and adsorbed Mo than Mn-oxides[47]. The operation of the Mn-Fe-oxyhydroxide shuttle is an unlikely reason for the low values at Tarfaya site 57. Although FeP/FeHR fluctuates around the ferruginous/anoxic threshold during E2, there is no distinct covariation between FeP/FeHR < 0.7 and low δ^{98}Mo. Furthermore, the operation of Mn-Fe-oxyhydroxide shuttle should result in high Mo EFs coinciding with low U EFs[31], which is not the case during E2 (Fig. 7).

3. Locally weakly euxinic bottom water

In this interval (53.12 and 52.10 m), both Re/Mo and Cr/Mo show a consistent inverse relationship with δ^{98}Mo (Fig 4). The combined evidence of high Re/Mo and Cr/Mo ratios and relatively low Mo enrichment factors (Fig. 4), argue for low sulfide availability in the water column, implying that Mo isotope compositions do not record a seawater signal. During the weakly euxinic conditions, formation of intermediate thiomolybdates (MoO_3S^{2-} to $MoOS_3^{2-}$) is favoured[38,39]. The transfomation of molybdate to various thiomolybdates is possibly connected with a substantial negative fractionation during each sulfidation step[40,48]. Furthermore, the uptake of intermediate thiomolybdates is non-quantitative and thus results in isotopic fractionations from global seawater of up to -2.9‰ (Fig. 1)[41].

4. Non-ideal conditions for sufficient Mo-Fe-S formation

The Helz et al. (2011)[49] revised Mo model suggests that an only an interplay of ideal pH, H_2S and reactive Fe availability can result in a quantitative scavenging of Mo, enabling the preservation of the seawater δ^{98}Mo. A more alkaline pH of > 8 would inhibit removal of Mo, due to higher solubility of the Mo-Fe-S phases at higher pH. Sulphate reducing conditions typically drive the pH to ~ 7, which is favourable for Mo removal to the sediment. Sufficient reactive Fe is important in order to maintain Mo-Fe-S saturation. Finally, a non-intuitive but evident outcome of the Helz et al. (2011)[49] model is that although H_2S needs to be sufficiently high (>11 μm), a large excess of sulfide would reverse the efficient Mo removal.

We assume that the first two points are sustained for sufficient removal of Mo. It is unlikely that the pH would have been higher during more sulfidic conditions through E2 than during the ferruginous intervals. Reactive Fe would have been sufficient during both sulfidic and ferruginous intervals[25]. However, it should be noted that lower concentrations of highly reactive Fe coincide with low δ^{98}Mo during this period. Weakly euxinic conditions are feasible, as explained in the previous point. However, if the high Re/Mo and Cr/Mo are not indicative of weakly sulfidic conditions and rather reflect the overall global preferential removal of Mo to the sediment over Re and Cr, then H_2S may have been extremely high at Tarfaya during E2 and according to the revised Helz et al. (2011)[49] model Mo would not have been quantitatively scavenged to reflect the seawater δ^{98}Mo.

3.3.2. II and III: constant value of ~ 0.6 and shift to ~ 1.1‰

The higher and relatively constant δ^{98}Mo in the upper and lower sections, with an average value of 0.6 ± 0.1‰ and an intermittent increase to 1.1‰, coincide with low Re/Mo and Cr/Mo ratios and the highest Mo enrichment factors, suggesting that dissolved sulfide concentrations were at a maximum during these intervals (Fig. 4). The low variability in δ^{98}Mo across ferruginous intervals is likely due to significant drawdown of Mo during short-lived episodes of euxinia, and/or due to highly euxinic porewaters, which were open to Mo

343 exchange with the water column [22,25]. Thus, the upper and lower sections of Tarfaya site S57
344 may represent times of near-quantitative scavenging of Mo from the water column.
345 Nevertheless "non-ideal" conditions for Mo scavenging, as presented by Helz et al. (2011)[49]
346 could be also operating during these intervals and thus the highest δ^{98}Mo may represent the
347 closest estimate to the global seawater value. It is also yet to be proven whether a "global"
348 δ^{98}Mo signal existed during OAE2.
349
350 ***3.4 Implications for the global Mo reservoir***
351 The low δ^{98}Mo of ~0.6‰ to 1.1‰ recorded at Tarfaya has the potential to represent
352 the global palaeo-seawater value. This implies a large decrease in the Mo reservoir during
353 OAE2 via an increase in euxinic Mo drawdown. The low Mo/TOC values recorded in euxinic
354 sections could therefore have been the result of a decrease in global Mo concentrations
355 during the event[50]. Regarding the evidence for expanded sulfidic conditions prior to OAE2
356 together with the possible drawdown of redox sensitive elements[4,8,9], seawater δ^{98}Mo would
357 have been lower than today well before the onset of OAE2 and would have reached a
358 minimum during the peak of the event.
359 To provide further insight into whether δ^{98}Mo values of 0.6‰ and 1.1‰ may reflect
360 seawater signatures at different times, we employed a 1-box model that links the relative
361 burial of Mo into three sinks (oxic, anoxic and euxinic) to the areal extent of each redox
362 environment at different seawater δ^{98}Mo values. In the direct feedback model, the residence
363 time of Mo in seawater is calculated by a burial forcing function, in which the modern areal
364 extent of each sink and the removal fluxes to each sink are scaled to the ancient seafloor
365 coverage.
366 At steady state, the sum of the Mo fluxes to the ocean ($F_{SOURCES}$) is equal to the sum of
367 the Mo outputs (F_{SINKS}) to various sinks[51,52]. The residence time (τ) of Mo in seawater is then

described by the global marine Mo inventory (M) in proportion to all source or sink fluxes (F):

$$\frac{M}{\tau} = F_{SOURCES} = F_{SINKS}$$

The total Mo flux to, or removal from, the ocean is the product of the areal extent (A) of each sink (i) and the burial rate (R) into each sink:

$$F(i) = A(i) \cdot R(i)$$

The Mo outflux from seawater is subdivided into three sinks: an oxic sink (f_{ox}), an intermediate sink, comprising reducing conditions with H_2S build-up in sediment porewaters and weakly euxinic environments (less than 11 µM H_2S), termed f_{red}, and a euxinic sink (f_{eux}) with bottom water H_2S_{aq} >11 µM. The sum of all fractional fluxes makes up the total Mo sink:

$$F_{SINKS} = f_{ox} + f_{red} + f_{eux}$$

The respective Mo isotope signatures (δ_{ox}, δ_{red} and δ_{eux}) are tied into a Mo isotope mass balance equation, where δ^{98}Mo of the sum of the sources (δ_{INPUT}) are equal to the sinks:

$$\delta_{INPUT} = f_{ox} \cdot \delta_{ox} + f_{red} \cdot \delta_{red} + f_{eux} \cdot \delta_{eux}$$

Thus, oceanic δ^{98}Mo is defined as :

$$\delta_{SW} = \delta_{INPUT} - f_{ox} \cdot \delta_{ox} + f_{red} \cdot \delta_{red} + f_{eux} \cdot \delta_{eux}$$

To calculate the Cretaceous (K) Mo budget, a self-regulated direct feedback function is applied, where the Mo burial rates vary in proportion to the Mo inventory (first-order process):

$$R(i)_K = \frac{R(i) \cdot M}{M_K}$$

We can describe the rate of change of the Mo inventory as:

$$\frac{dM}{dt} = F_{SINKS} - \frac{M}{\tau}$$

In the burial forcing function the modern areal extent of each sink is scaled back to the Cretaceous areal extent to receive the Cretaceous Mo response time:

$$\frac{\tau}{\tau_{(K)}} = \frac{f_{ox} \cdot A_{ox_{(K)}}}{A_{ox}} + \frac{f_{red} \cdot A_{red_{(K)}}}{A_{red}} + \frac{f_{eux} \cdot A_{eux_{(K)}}}{A_{eux}}$$

Rivers are by far the biggest source of dissolved Mo to the ocean and account for at least 90% of the influx[53], with low-temperature hydrothermal inputs accounting for the remainder[54,55]. As the latter input is poorly constrained in magnitude and Mo isotope composition, we disregard this source of Mo to the ocean. Recently, the riverine Mo flux to the ocean has been reassessed as 2.96 x 10^7 kg a^{-1} [34], which is ~ 1.6 fold higher than previously assumed. With a total seawater mass of 1.37 x 10^{21} kg (considering a seawater density of 1.028 kg L^{-1}) and a Mo concentration of 104 nM kg^{-1}, we calculate a total marine Mo inventory of 1.37 x 10^{13} kg and an oceanic Mo residence time of ~460 ka (similar to previous calculation of 440 ka[34]), which is almost half of the residence time quoted in earlier studies (700 to 800 ka)[56,57].

At present, oxic sediments are assessed to cover 96 to 97% of the ocean floor[33] whilst A_{red} and A_{eux} are estimated at 1% and 0.05%, respectively[50,58]. We hence subdivide the total seafloor of 3.6x10^8 km^2 into three redox regimes, with A_{ox} = 97 %, A_{red} = 1 % and A_{eux} = 0.05 % of the ocean floor. For the model, the sum of the total seafloor coverage is kept constant.

At steady state, a higher input of Mo to the ocean requires a higher Mo output flux and thus a higher burial rate. Previously, modern Mo burial rates were estimated at r_{ox} = 0.002 µg cm^{-2} a^{-1}, r_{red} = 0.250 µg cm^{-2} a^{-1} and r_{eux} = 1.27 µg cm^{-2} a^{-1} [50,58]. To balance the budget we scale the rates up by a factor of ~ 1.6 (equivalent to the increase in the new riverine Mo flux), resulting in r_{ox} = 0.003 µg cm^{-2} a^{-1}, r_{red} = 0.4 µg cm^{-2} a^{-1} and r_{eux} = 1.8 µg cm^{-2} a^{-1}. These rates are consistent with the current knowledge of Mo accumulation rates in modern environments (Table S2). However, these burial rates may be exaggerated for the deep ocean, as the estimates are mainly based on data for shelf deposits. Nevertheless, we take these to be the average burial rates for each of the redox environments.

For the modern Mo isotope budget, we apply measured offsets (the difference in δ^{98}Mo between measured modern sediment and seawater values) to the modern seawater

415 δ^{98}Mo value of 2.09‰[28,43]. In oxic enviroments, δ^{98}Mo is mainly attributed to
416 ferromanganese crusts and nodules, with a well-established offset (δ_{OX}) of -3‰ (Fig. 1). In
417 highly sulfidic environments, sedimentary δ^{98}Mo is slightly offset from global seawater (Fig.
418 1) and we therefore apply a small offset of -0.05‰ for δ_{EUX}[59]. A relatively constant isotopic
419 fractionation relative to seawater of about -0.8‰ (renormalized to NIST SRM 3134) was
420 proposed to be driven by diagenesis beneath low oxygen to anoxic, non-sulfidic bottom
421 waters[42], where the sediment porewaters become sulfidic (Fig. 1). To include the weakly
422 euxinic sinks, we apply a higher offset of –0.9‰ for the intermediate sink (δ_{RED}). The average
423 modern δ^{98}Mo value of dissolved riverine Mo is about 0.4‰ (renormalized to NIST SRM
424 3134), based on rivers that represent ~22% of the global river discharge[43]. We assume a
425 constant riverine Mo flux and its isotopic composition, although these may have been offset
426 in the past[44,60].

427 For the modern burial rates and seafloor coverages for each sink, we calculate the
428 fraction of Mo deposited in each sink of f_{OX} = 0.41, f_{RED} = 0.48 and f_{EUX} = 0.11, which results in
429 a consistent value of 2.07‰ for modern seawater. The fluxes fall into the range of the
430 previously calculated Mo budget of 25 to 55% for oxic deposition, 45 to 70% for
431 suboxic/anoxic/sulfidic at depth deposition, and 5 to 15% for the euxinic sink[20,42,50,58]. For
432 the modelling of past fluxes, we disregarded unlikely cases where the oxic and euxinic end-
433 member sinks are dominant in comparison to the intermediate sink[21,40].

434 Figure 8A displays the solution space for the possible combinations of A_{eux} and A_{ox}
435 (A_{red} is not displayed), resulting in different seawater δ^{98}Mo values and response times (τ).
436 The modelled residence times should be regarded as minimum values, because we mainly
437 employ average burial rates reported for shelf environments, thus overestimating the burial
438 rates of the deep ocean. Seawater δ^{98}Mo values of 1.1 ± 0.1‰ and 0.6 ± 0.1‰ are obtained
439 for various combinations that feature different areal extents for each sink (Fig. 8). Model
440 results hence provide a range of possible Mo residence times from 7 to 191 ka for δ^{98}Mo = 1.1

441 ± 0.1‰, and from 3 to 62 ka for δ^{98}Mo = 0.6 ± 0.1‰. According to the model, a change from
442 ~0.6‰ to ~1.1‰ within ~20 to 25 ka (corresponding to 53.1 to 51.7 m depth in the S57
443 core) is therefore possible. Constraints on the exact timing and rate of change of the seawater
444 δ^{98}Mo value from 0.6 to 1.1‰ (from F2 to F3) are not available, as it is unlikely that seawater
445 δ^{98}Mo was recorded across this interval (see 3.3.1). The increase of the global seawater value
446 during peak OAE2 is, however, counterintuitive, as it requires a decrease in the area of anoxic
447 and mainly euxinic seafloor.

448 Available chronological constraints for the Tarfaya section provide a time span of ~3
449 to 4 ka for the decrease in δ^{98}Mo from 1.1 to 0.6‰ at ~51.6 to 51.4 m, close to the modern
450 average ocean mixing time of ~1.5 ka (Sarmiento and Gruber, 2006). The model predicts that
451 to drive the δ^{98}Mo response time to less than ~10 ka at a δ^{98}Mo value of 1.1 ± 0.1‰, less than
452 30% of the global seafloor would need to have oxygenated bottom water (Fig 8). Whether
453 such a scenario is feasible is debated. A near-global spread of anoxia has been suggested for
454 OAE2[3,11]. Further support comes from a recent modelling study, which suggests that >90% of
455 the deep ocean, excluding the Arctic and Southern oceans, would have been anoxic during
456 times of peak CO_2 (OAE2) and excess phosphate supply[61]. However, a less extreme spread of
457 anoxia during OAE2 is evidenced by some intermittent occurrences of oxic bottom water
458 during the event[6,22,37] and possibly even widespread oxic depositional conditions in the
459 Pacific Ocean[63]. In summary, we conclude that such a rapid decrease in the global δ^{98}Mo
460 during OAE2 is highly unlikely.

461 A rapid change from a seawater value of 1.1‰ to 0.6‰ would only have been
462 possible if Mo was heterogeneously distributed across the different Cretaceous ocean basins
463 and possibly between deep, intermediate and shallow water bodies as a consequence of a
464 small Mo reservoir. If correct, the δ^{98}Mo values of 0.6 and 1.1‰ at Tarfaya would reflect the
465 Mo isotope signature of a local water mass. Westermann et al. (2014)[22] recently reported
466 δ^{98}Mo of ~ 0.8‰ (recalculated to NIST SRM 3134) during OAE2 at site DSDP 367 (Fig 2) and

suggested that these reflect global seawater. This value would therefore represent the δ^{98}Mo of the deep Cape Verde water.

There is evidence of less reducing conditions during OAE2[6,22] where the light Mo isotopes were drawn down from seawater (e.g. site ODP 1276)[22], thus increasing the ambient seawater δ^{98}Mo value. Water circulation and water mass mixing would still have been operational during OAE2[64]. Consequently, the ambient seawater Mo composition could have varied throughout the Cretaceous ocean during OAE2, in response to variable rates of seawater renewal that were driven by more localised changes in runoff and water circulation, which drove the changes in the Tarfayan seawater δ^{98}Mo.

Alternatively, it is possible that "non-ideal" conditions were prevalent with regard to Mo-Fe-S scavenging at Tarfaya S57. Most of the δ^{98}Mo record could either be driven by concentrations of H_2S that were either too low or too high, as proposed by Helz et al. (2011)[49] (see section 3.1.1). In this case, the highest δ^{98}Mo of 1.1 ‰ (equivalent to 1.4 ‰ on the Roch-Mo2 scale[28]) would be closest to a global seawater signal. A clear indication can only be supported by further Mo isotope evidence from other Tarfaya sections in combination with water circulation indicators (e.g. Nd isotopes).

4. Conclusions

The new high-resolution δ^{98}Mo record from the Late-Cretaceous shelf off NW-Africa at Tarfaya emphasises the need for a combination of redox proxies to differentiate between the potential for quantitative and non-quantitative scavenging of Mo in seawater. This information is essential to resolve whether sedimentary δ^{98}Mo records the overlying δ^{98}Mo seawater signal. Redox proxy records from Tarfaya site S57 and Mo-burial modelling suggest that seawater δ^{98}Mo may have varied during OAE2 from about 0.6 to 1.1‰. The rapid changes in seawater δ^{98}Mo can only be reconciled by heterogeneous oceanic δ^{98}Mo and Mo

concentrations during OAE2. Alternatively, a true δ^{98}Mo signal was not established at Tarfaya site 57, and 1.1‰ represents the closest value to seawater δ^{98}Mo.

Low Mo/TOC ratios in several regions of the proto-North Atlantic in comparison to other oceanic basins argue for partial restriction of the proto-North Atlantic deep water in the Late-Cretaceous. However, the inferred restriction cannot account for the 2 to 8 times lower Mo/TOC ratios of the proto-North Atlantic, compared to the modern Black Sea, and the overall low Mo accumulation rate, as observed in the Tethyan and South Atlantic regions. If true, then the low δ^{98}Mo values are consistent with enhanced drawdown of Mo through expansion of euxinic bottom waters across large parts of the global ocean during OAE2. Taken together, the decline in Mo/TOC values in the Tarfaya and Demerara Rise sites during the onset of the OAE2, and the Mo isotope evidence for a low and possibly heterogeneous seawater δ^{98}Mo, point towards a decrease in the global marine concentration of Mo during OAE2, with enhanced euxinic Mo drawdown under expanded sulfidic conditions. As such, care should be exercised when utilising Mo concentrations alone as an indicator of water column euxinia during OAE2 and maybe other OAEs. It is also possible that other redox sensitive trace elements were extensively buried during expanded and prolonged euxinia, and hence were depleted in the water column.

Acknowledgements

This work was supported by a Natural Environment Research Council grant to TG (NERC, NE/G01499X/2). TW acknowledges support from a Royal Society Wolfson Research Merit Award. We greatly thank A. Forster and M. Kuypers for kindly supplying raw data. We greatly appreciate the very fast review and editing of the manuscript by Chris Pearce, Karl Föllmi, an anonymous reviewer and Derek Vance (editor), which very much helped to improve the contents.

518 **Figure and Table Captions**

519 Figure 1 The main oceanic Mo sources and sinks, and their isotopic compositions. Note that
520 δ^{98}Mo has been renormalised to NIST SRM 3134, according to Goldberg et al. (2013)[28].
521 Narrow boxes represent the reported data range for each environment; wide boxes represent
522 areas of data concentration. δ^{98}Mo values compiled from Vögelin et al. (2012 and references
523 therein)[60] and Goldberg et al. (2012, 2013, and references therein)[28,47].

524

525 Figure 2 Continental reconstruction for 94 Ma (modified from Forster et al., 2008), with the
526 study site (Tarfaya S57) and other locations discussed in this study. Light grey areas
527 represent land and middle grey areas represent flooded continental plates. Thin black lines
528 outline present day coastlines.

529

530 Figure 3 Total organic carbon (δ^{13}C) from Tsikos et al., (2004)[23] and division into δ^{13}C phases
531 A and B, with indication of first occurrence of *R. cushmani*, after Kolonic et al. (2005)[8] for the
532 studied S57 Tarfaya section. Fe-speciation from Poulton et al. (2015)[25], with grey shaded
533 intervals representing ferruginous bottom water conditions, numbered F1 to F5, between
534 predominantly euxinic bottom water intervals, numbered E1 to E4.

535

536 Figure 4. Trace element enrichment factors (Mo, U, V, Cr and Re) and Mo/Re and Mo/Cr
537 ratios and δ^{98}Mo (relative to NIST SRM 3134) throughout the studied S57 Tarfaya section.
538 Mo, U and V concentrations are compared to oxic background values, as represented by Post-
539 Archean Average Shale (PAAS)[65], and are calculated as enrichment factors (EF =
540 $\text{element/Al})_{\text{sample}}/(\text{element/Al})_{\text{PAAS}}$). Rhenium and Cr EFs are normalised to their crustal
541 values, with $\text{Re} = 0.06 \times 10^{-7}$ [14] and $\text{Cr} = 11 \times 10^{-4}$ [65], respectively. Ferruginous and euxinic
542 intervals are numbered F1 to F5 and E1 to E4, respectively.

543

Figure 5: TOC plotted against A: Mo, B: U and C: V. Dashed line represents Black Sea average Mo/TOC. Correlation between TOC and Mo is not particularly strong. This may be connected to the fact that Mo is associated both with pyrite and TOC and/or may depend on the type of organic matter.

Figure 6: Data from the study site (Tarfaya S57). Mo/TOC x 10^{-4} data from Kolonic et al. (2005)[8] and this study. Grey boxes represent the span of OAE2 and white boxes represent time period analysed in this study.

Figure 7. Mo and U systematics from Algeo & Tribovillard (2009)[31] and Tribovillard et al. (2012)[32]. At high Mo and U EFs (indicative of euxinic conditions) progressively greater enrichment of Mo over U (Mo:U > seawater) is considered to reflect unrestricted anoxic conditions (grey arrow), as Mo is constantly sourced from the open ocean. In semi-closed sulfidic water bodies, Mo burial overwhelms Mo resupply faster than U, resulting in Mo:U ratios that are smaller compared to seawater as EFs increase. A third process describes an enhanced export of aqueous Mo to the sediment via a metal oxyhydroxide particulate shuttle with little effect on U. This process is characterised by high Mo EFs and low U EFs, but Mo:U ratios that exceed the seawater value by up to a factor of 3. Black and grey symbols represent EFs from this study and white symbols represent EFs for black shales from the South Altantic site DSDP 603B (data from Forster et al., 2008[37]). Grey symbols are data from period E2. Diagonal lines represent multiples of the Mo:U present day seawater.

Figure 8. A. Solution space of the box model. To maintain visibility, a limited number of possible combinations is displayed. White lines represent a specific areal extent of bottom water euxinia (eux) and grey lines represent a specific areal extent for oxic (ox) bottom water. Areal extent for reducing (red) conditions is not shown. Different combinations of residence times (τ) and seawater δ^{98}Mo are possible within the solution space. B. Mo burial is

subdivided into three sinks: an oxic sink (ox), an intermediate sink (red), comprising reducing conditions with H_2S and build-up in sediment porewaters and weakly euxinic environments (less than 11µM H_2S_{aq}), and a euxinic sink (eux) with bottom water H_2S_{aq} >11µM. Possible combinations of seafloor area (in %) representing these sinks along with the respective Mo residence time are displayed for δ^{98}Mo seawater values of 1.1 ± 0.1‰ and 0.6 ± 0.1‰.

Table 1: Overview of Mo/TOC values during and prior to OAE2.

Supplement

Supplement 1.

Table S1: δ^{98}Mo and trace element data

Table S2: Mo accumulation rates in modern settings at different oxygen and H_2S content.

References

1. Friedrich, O., Norris, R. D., Erbacher, J., 2012. Evolution of middle to Late Cretaceous oceans–A 55 m.y. record of Earth's temperature and carbon cycle, Geology 40, 107–110.
2. Jenkyns, H.C., 2010. Geochemistry of oceanic anoxic events. Geochemistry, Geophysics, Geosystems 11, doi:10.1029/2009GC002788.
3. Schlanger S.O., Jenkyns H.C., 1976. Cretaceous oceanic anoxic events: causes and consequences, Geol. Mijnb. 55 179–184.
4. Kuypers, M.M.M., Pancost, R.D., Nijenhuis, I.A., Sinninghe Damsté, J.S., 2002. Enhanced productivity led to increased organic carbon burial in the euxinic North Atlantic basin during the late Cenomanian oceanic anoxic event, Paleoceanography 17, PA1051, doi: 10.1029/2000PA000569.
5. Mort, H.P., Adatte, T., Föllmi, K.B., Keller, G., Steinmann, P., Matera, V. Berner, Z., Stuben, D, 2007. Phosphorus and the roles of productivity and nutrient recycling during oceanic anoxic event 2. Geology 35, 483–486.
6. Kuypers, M. M. M., Lourens, L. J., Rijpstra, W. I. C., Pancost, R. D., Nijenhuis, I. A., Sinninghe Damsté J. S., 2004. Orbital forcing of organic carbon burial in the proto-North Atlantic during oceanic anoxic event 2, Earth Planet. Sci. Lett. 228, 465–482.
7. Lüning, S., Wagner, T., Cota, L., Bari, G., Belhadj, Z. and Hauptmann, M., 2004. Integrated depositional model for the Cenomanian-Turonian organic-rich strata in North Africa. Earth Science Reviews 64, 51-117.
8. Kolonic, S., Wagner, T., Forster, A., Sinningh Damsté, J.S.,Walsworth-Bell, B., Erba, E., Turgeon, S., Brumsack, H.J., Chellai, E.H., Tsikos, H., Kuhnt, W., Kuypers, M.M.M., 2005. Black shale deposition on the northwest African Shelf during the Cenomanian/Turonian oceanic

anoxic event: Climate coupling and global organic carbon burial. Paleoceanography 20, PA1006, doi:10.1029/2003PA000950.
9. Hetzel, A., Böttcher, M.E., Wortmann, U.G. & Brumsack, H.-J., 2009. Paleo-redox conditions during OAE 2 reflected in Demerara Rise sediment geochemistry (ODP Leg 207) Palaeogeogr. Palaeoclimatol. Palaeoecol. 273, 302-328.
10. Lenniger, M., Nøhr-Hansen, H., Hills, L.V., Bjerrum, C.J., 2014. Arctic black shale formation during Cretaceous Oceanic Anoxic Event 2. Geology 42, 799-802.
11. Monteiro, F. M., Pancost, R. D., Ridgwell, A., Donnadieu, Y., 2013. Nutrients as the dominant control on the spread of anoxia and euxinia across the Cenomanian-Turonian oceanic anoxic event (OAE2): Model-data comparison. Paleoceanography 27, 1-17, PA4209, doi:10.1029/2012PA002351.
12. Wagner T, Hofmann P, Flögel S., 2013. Marine black shale and Hadley Cell dynamics: A conceptual framework for the Cretaceous Atlantic Ocean. Marine Petroleum Geology 43, 222-238.
13. Jiménez Berrocoso, A., MacLeod, K. G., Martin, E. E., Bourbon, E., Isaza Londoño, C., and Basak, C. 2010. Nutrient trap for the Late Cretaceous organic-rich black shales in the tropical North Atlantic. Geology 38, 1111–1114.
14. Crusius, J., Calvert, S., Pedersen, T., Sage, D., 1996. Rhenium and molybdenum enrichments in sediments as indicators of oxic, suboxic, and sulfidic conditions of deposition. Earth and Planetary Science Letters 145, 65–78.
15. Algeo, T.J., Maynard, J.B., 2004. Trace-element behaviour and redox facies in core shales of Upper Pennsylvanian Kansas-type cyclothems. Chemical Geology 206, 289-318.
16. Zheng, Y., Anderson, R.F., van Geen, A., Kuwabara, J., 2000. Authigenic molybdenum formation in marine sediments: A link to pore water sulphide in the Santa Barbara Basin. Geochimica et Cosmochimica Acta 64, 4165–4178.
17. Algeo, T.J., Lyons, T., 2006. Mo-total organic carbon covariation in modern anoxic marine environments: Implications for analysis of paleoredox and paleohydrographic conditions. Paleoceanography 21, doi:10.1029/2004PA001112.
18. McArthur, J.M., Algeo, T.J., van de Schootbrugge, B., Li, Q., Howarth, R.J., 2008. Basinal restriction, black shales, Re–Os dating, and the Early Toarcian (Jurassic) oceanic anoxic event. Paleoceanography 23, PA4217. doi:10.1029/2008PA001607.
19. Pearce, C.R., Cohen, A., Coe, A.L., Burton, K.W., 2008. Molybdenum isotope evidence for global ocean anoxia coupled with perturbations to the carbon cycle during the Early Jurassic. Geology 36, 231-234.
20. Dickson, A.J., Cohen, A.S. Coe, A.L., 2012. Seawater oxygenation during the Paleocene-Eocene Thermal. Geology 40, 639-642.
21. Kendall B., Gordon, G. W., Poulton S. W. and Anbar A. D., 2011. Molybdenum isotope constraints on the extent of late Paleoproterozoic ocean euxinia. Earth Planet. Sci. Lett., 307, 450-460.
22. Westermann, S., Vance, D., Cameron, V., Archer, C., Robinson, S.A. 2014. Heterogeneous oxygenation states in the Atlantic and Tethys oceans during Oceanic Anoxic Event 2. Earth and Planetary Science Letters 404, 178–189.
23. Tsikos, H., Jenkyns, H.C., Walsworth-Bell, B., Petrizzo, M.R., Forster, A., Kolonic, S., Erba, E., Premoli Silva, I., Baas, M., Wagner, T., Sinninghe Damsté, J.S., 2004. Carbon isotope stratigraphy recorded by the Cenomanian-Turonian Oceanic Anoxic Event: correlation and implications based on three key localities. Journal of the Geological Society, London 161, 711–719.
24. Mort, H.P., Adatte, T., Keller, G., Bartels, D., Föllmi, K.B., Steinmann, P., Berner, Z., Chellai, E.H., 2008. Organic carbon deposition and phosphorus accumulation during Oceanic Anoxic Event 2 in Tarfaya, Morocco. Cretaceous Research 29, 1008–1023.
25. Poulton, S.W., Henkel, S., März, C., Urquhart, H., Flögel, S., Kasten, S., Sinninghe-Damsté, J.S. and Wagner, T. (2015) A continental-weathering control on orbitally driven redox-nutrient cycling during Cretaceous Oceanic Anoxic Event 2. Geology, in press.

661 26. Kuhnt, W., Holbourn, A., Gale, A., Chellai, E.H., and Kennedy, W.J., 2009, Cenomanian
662 sequence stratigraphy and sea-level fluctuations in the Tarfaya Basin (SW Morocco):
663 Geological Society of America Bulletin, v. 121, p. 1695–1710.
664 27. Meyers, S.R., Sageman, B.B. & Arthur, M.A., 2012. Obliquity forcing of organic matter
665 accumulation during Oceanic Anoxic Event 2. Paleoceanography 27, PA3212,
666 doi:10.1029/2012PA002286.
667 28. Goldberg, T., Gordon, G., Izon, G., Archer, C., Pearce, C.R., McManus, J., Anbar, A.,
668 Rehkämper, M., 2013. Resolution of inter-laboratory discrepancies in Mo isotope data: An
669 intercalibration. J Anal. Atom. Spectrom. 28, 724.
670 29. Kuhnt, W., Luderer, F., Nederbragt, A., Thurow, J., Wagner, T., 2005. Orbital scale
671 record of the late Cenomanian-Turonian Oceanic Anoxic Event (OAE 2) in the Tarfaya Basin
672 (Morocco). International Journal of Earth Sciences 94, 147–159.
673 30. Poulton S.W., Canfield D.E, 2011. Ferruginous conditions: A dominant feature of the
674 ocean through Earth's history. Elements 7, 107-112.
675 31. Algeo, T.J., Tribovillard, N., 2009. Environmental analysis of paleoceanographic
676 systems based on molybdenum–uranium covariation. Chemical Geology 268, 211–225.
677 32. Tribovillard, N., Algeo, T.J., Lyons, T.W., Riboulleau, A., 2012. Analysis of marine
678 environmental conditions based on molybdenum–uranium covariation—Applications to
679 Mesozoic paleoceanography. Chemical Geology 324-325, 46-58.
680 33. Morford J.L., Emerson S., 1999. The geochemistry of redox sensitive trace metals in
681 sediments. Geochim. Cosmochim. Acta 63, 1735–1750.
682 34. Miller, A.C., Peucker-Ehrenbrink, B., Walker, B.D., Marcantonio, F., 2011. Re-assessing
683 the surface cycling of molybdenum and rhenium. Geochimica et Cosmochimica Acta 75,
684 7146–7179.
685 35. Martin, E. E., MacLeod, K. G., Jiménez Berrocoso, A., Bourbon, E., 2012. Water mass
686 circulation on Demerara Rise during the Late Cretaceous based on Nd isotopes. Earth and
687 Planetary Science Letters 327-328, 111–120.
688 36. van Helmond, N. A. G. M., Ruvalcaba Baroni, I., Sluijs, A., Sinninghe Damste, J.S., Slomp,
689 C.P., 2014. Spatial extent and degree of oxygen depletion in the deep proto-North Atlantic
690 basin during Oceanic Anoxic Event 2. Geochemistry, Geophysics, Geosystems, 15, 4254-4266.
691 37. Forster, A., Kuypers, M.M.M., Turgeon, S.C., Brumsack, H.-J., Petrizzo, M.R., Sinninghe
692 Damsté, J. S. 2008. The Cenomanian/Turonian oceanic anoxic event in the South Atlantic:
693 New insights from a geochemical study of DSDP Site 530A. Palaeogeography,
694 Palaeoclimatology, Palaeoecology 267, 256–283.
695 38. Helz, G.R., Vorlicek, T.P., Kahn, M.D., 2004. Molybdenum scavenging by iron
696 monosulfide. Environmental Science & Technology 38, 4263-4268.
697 39. Vorlicek, T.P., Kahn, M.D., Kasuza, Y., Helz, G.R., 2004. Capture of molybdenum in pyrite
698 forming sediments: role of ligand-induced reduction by polysulfides. Geochimica et
699 Cosmochimica Acta 68, 547–556.
700 40. Dahl, T.W., Anbar, A.D., Gordon, G.W, Rosing, M.T., Frei, R., Canfield, D.E., 2010. The
701 behaviour of molybdenum and its isotopes across the chemocline and in the sediments of
702 sulfidic Lake Cadago, Switzerland. Geochimica et Cosmochimica Acta 74, 144-163.
703 41. Neubert, N., Nägler, T.F., Böttcher, M.E., 2008. Sulphidity controls molybdenum
704 isotope fractionation into euxinic sediments: Evidence from the modern Black Sea. Geology
705 36, 775-778.
706 42. Poulson-Brucker, R.L., McManus, J., Poulton, S.W., 2012. Molybdenum isotope
707 fractionations observed under anoxic experimental conditions. Geochemical Journal 46, 201-
708 209.
709 43. Archer, C., Vance, D., 2008. The isotopic signature of the global riverine molybdenum
710 flux and anoxia in the ancient oceans. Nature Geoscience 1, 597-600.
711 44. Neubert N., Heri A. R., Voegelin A. R., Nägler T. F., Schlunegger F. and Villa I. M., 2011.
712 The molybdenum isotopic composition in river water: Constraints from small catchments.
713 Earth Planet. Sci. Lett., 304, 180-190.

714 45. Barling, J., Anbar, A.D, 2004. Molybdenum isotope fractionation during adsorption by
715 manganese oxides. Earth and Planetary Science Letters 217, 315-329.
716 46. Herrmann A. D., Kendall B., Algeo T. J., Gordon G. W., Wasylenki L. E. and Anbar A. D.,
717 2012. Anomalous molybdenum isotope trends in Upper Pennsylvanian euxinic facies:
718 Significance for use of d98Mo as a global marine redox proxy. Chemical Geology 324–325,
719 87–98.
720 47. Goldberg T., Archer, C., Vance, D., Thamdrup, B., McAnena, A., Poulton, S.W., 2012.
721 Controls on Mo isotope fractionations in a Mn-rich anoxic marine sediment, Gullmar Fjord,
722 Sweden. Chemical Geology 296-297, 73–82.
723 48. Tossell, J.A. (2005) Calculating the partitioning of the isotopes of Mo between oxidic
724 and sulphidic species in aqueous solution. Geochimica et Cosmochimica Acta 69, 2981–2993.
725 49. Helz, G.R., Bura-Nakić, E., Mikac, N., Ciglenečki, I., 2011. New model for molybdenum
726 behavior in euxinic waters. Chemical Geology 284, 323–332.
727 50. Scott C., Lyons T.W., Bekker A., Shen Y., Poulton S.W., Chu X., Anbar A.D., 2008. Tracing
728 the stepwise oxygenation of the Proterozoic ocean: Nature 452, 456–459.
729 51. Rodhe, H., 1992. Modeling biogeochemical cycles, In: Butcher, S.S., et al. (eds), Global
730 biogeochemical cycles: San Diego, Academic Press, p. 55–72.
731 52. Sarmiento, J.L., Gruber, N., 2006. Ocean Biogeochemical Dynamics. Princeton
732 university press, New Jersey, USA. 503 pp.
733 53. Martin, J. M. & Meybeck, N., 1979. Elemental mass-balance of material carried by
734 major world rivers. Marine Chemistry 7, 173-206.
735 54. McManus, J., Berelson, W.M., Severmann, S., Poulson, R.L., Hammond, D.E.,
736 Klinkhammer, G.P., Holm, C., 2006. Molybdenum and uranium geochemistry in continental
737 margin sediments: Paleoproxy potential. Geochimica et Cosmochimica Acta 70, 4643–4662.
738 55. Wheat, C., G., Mottl, M.J., and Rudnicki, M., 2002. Trace element and REE composition
739 of a low-temperature ridge-flank hydrothermal spring. Geochimica et Cosmochimica Acta 66,
740 3693–3705.
741 56. Emerson S., Huested S., 1991. Ocean anoxia and the concentration of molybdenum and
742 vanadium in seawater. Mar. Chem. 39, 177–196.
743 57. Algeo, T.J., 2004. Can marine anoxic events draw down the trace-element inventory of
744 seawater? Geology 32, 1057–1060.
745 58. Dahl, T.W., Canfield, D.E., Rosing, M.T., Frei, R., Gordon, G.W, Knoll, A.H., Anbar, A.D.,
746 2011. Molybdenum evidence for expansive sulfidic water masses in ~750 Ma oceans. Earth
747 and Planetary Science Letters 311, 264-274.
748 59. Chen, X., Ling, H.F, Vance, D. Shields-Zhou, G.A., Zhu, M., Poulton, S. W., Och, L.M., Jiang,
749 S-Y, Li, D., Cremonese, L., Archer, C., 2015. Rise to modern levels of ocean oxygenation
750 coincided with the Cambrian radiation of animals. Nature Communications 6, 7142, DOI:
751 10.1038/ncomms8142.
752 60. Vögelin A. R., Nägler T. F., Pettke, T., Neubert, N, Steinmann, M., Pourret, O, Villa I. M.,
753 2012. The impact of igneous bedrock weathering on the Mo isotopic composition of stream
754 waters: Natural samples and laboratory experiments. Geochimica et Cosmochimica Acta 86,
755 150–165.
756 61. Flögel, S., Wallmann, K., Kuhnt, W., 2011. Cool episodes in the Cretaceous — Exploring
757 the effects of physical forcings on Antarctic snow accumulation. Earth and Planetary Science
758 Letters 307, 279–288.
759 62. Westermann S., Caron, M., Fiet, N., Fleitmann, D., Matera, V., Adette, T., Foellmi, KB.,
760 2010. Evidence for oxic conditions during oceanic anoxic event 2 in the northern Tethyan
761 pelagic realm. Cretaceous Research 31, 500-514.
762 63. Hay, W.W., et al., 1999. An alternative global Cretaceous paleogeography, in Evolution
763 of the Cretaceous Ocean/Climate System, edited by E. Barrera and C. Johnson, Spec. Pap. Geol.
764 Soc. Am., 332, 1–47.

	Site	pre-OAE2 Mo/TOC	OAE2 Mo/TOC	Reference
within proto North Atlantic	Site S57, Tarfaya Basin	4×10^{-4}	1×10^{-4}	this study; Kolonic et al. (2005)
	Site 1258 and 1260, ODP Leg 207, Demerara Rise	9×10^{-4}	2×10^{-4}	Hetzel et al. (2009)
	603B, DSDP Leg 93, Off Cape Hatteras	$*9 \times 10^{-4}$	3×10^{-4}	Kuypers et al. (2004); van Helmond (2014)
	Site 367, DSDP Leg 41, Cape Verde Basin	11×10^{-4}	5×10^{-4}	Westermann et al. (2014)
	ODP 1276, Newfoundland Basin	n.a.	2×10^{-4}	Westermann et al. (2014)
	Site 368, DSDP Leg 43, Central Bermuda Rise	$*29 \times 10^{-4}$	5×10^{-4}	van Helmond et al. (2014)
	Site 641, Leg 103, Galicia Bank	$*98 \times 10^{-4}$	300×10^{-4}	van Helmond et al. (2014)
outside proto North Atlantic	Calabianca, western Tethys	n.a.	2×10^{-4}	Tribovillard et al. (2011)
	Bottaccione, western Tethys	n.a.	4×10^{-4}	Tribovillard et al. (2011)
	Contessa, western Tethys	n.a.	3×10^{-4}	Westermann et al. (2014)
	Furlo, western Tethys	n.a.	9×10^{-4}	Westermann et al. (2014)
	DSDP 560, Angola Basin	63×10^{-4}	12×10^{-4}	Forster et al. (2008)

n.a = no data or no inication of seawater redox conditions
* not representative, based on too few values

Fig 1

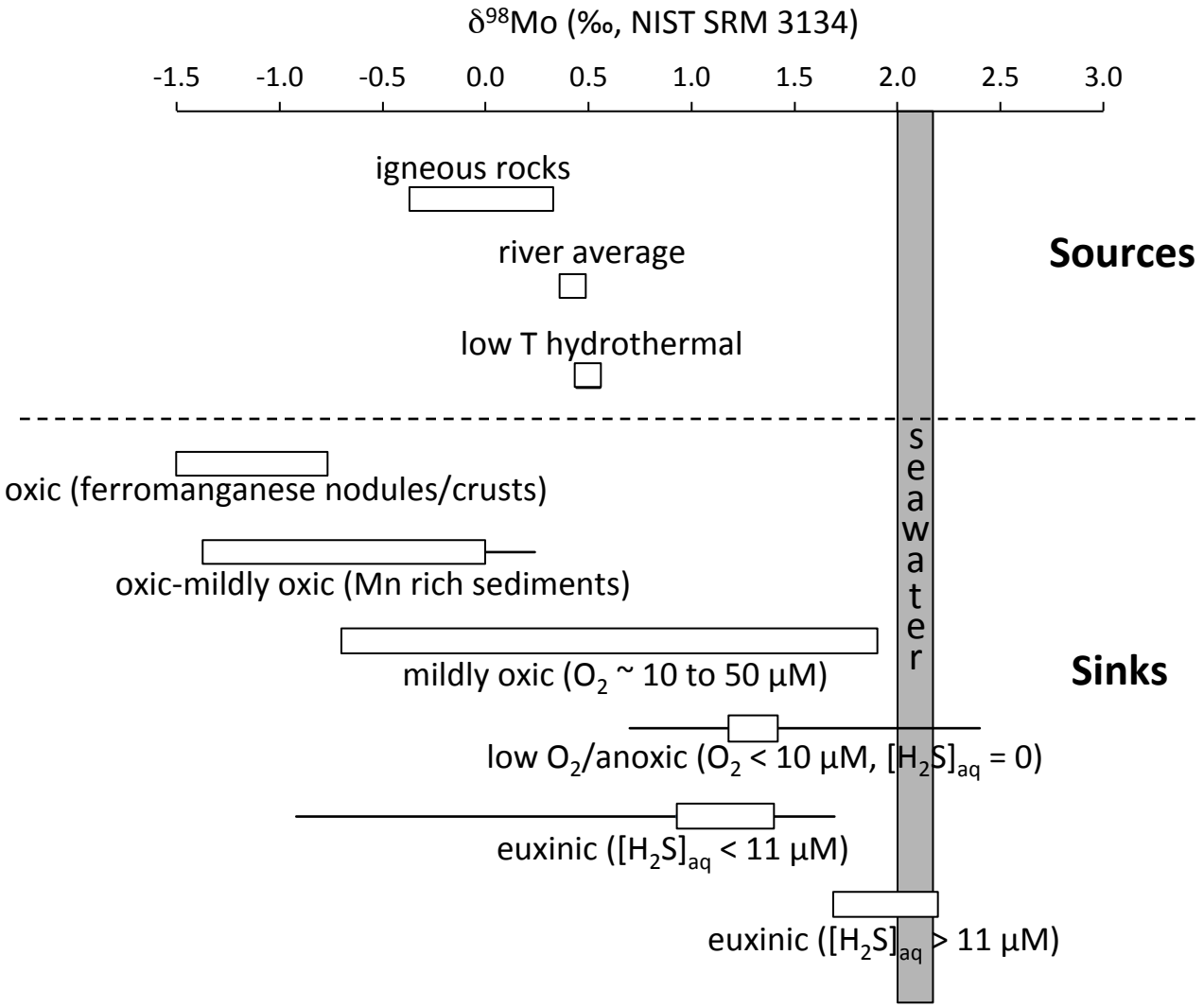

δ98Mo (‰, NIST SRM 3134)
-1.5
-1.0
-0.5
0.0
0.5
1.0
1.5
2.0
2.5
3.0
igneous rocks
river average
low T hydrothermal
Sources
seawater
oxic (ferromanganese nodules/crusts)
oxic-mildly oxic (Mn rich sediments)
mildly oxic (O2 ~ 10 to 50 µM)
Sinks
low O2/anoxic (O2 < 10 µM, [H2S]aq = 0)
euxinic ([H2S]aq < 11 µM)
euxinic ([H2S]aq > 11 µM)

Fig. 2


DSDP 603B
ODP 1276
Bottaccione/
Furlo/La Contessa
ODP 641
DSDP 368
Tarfaya S57
Calabianca
DSDP 367
Demerara
DSDP 530A

Figure 4

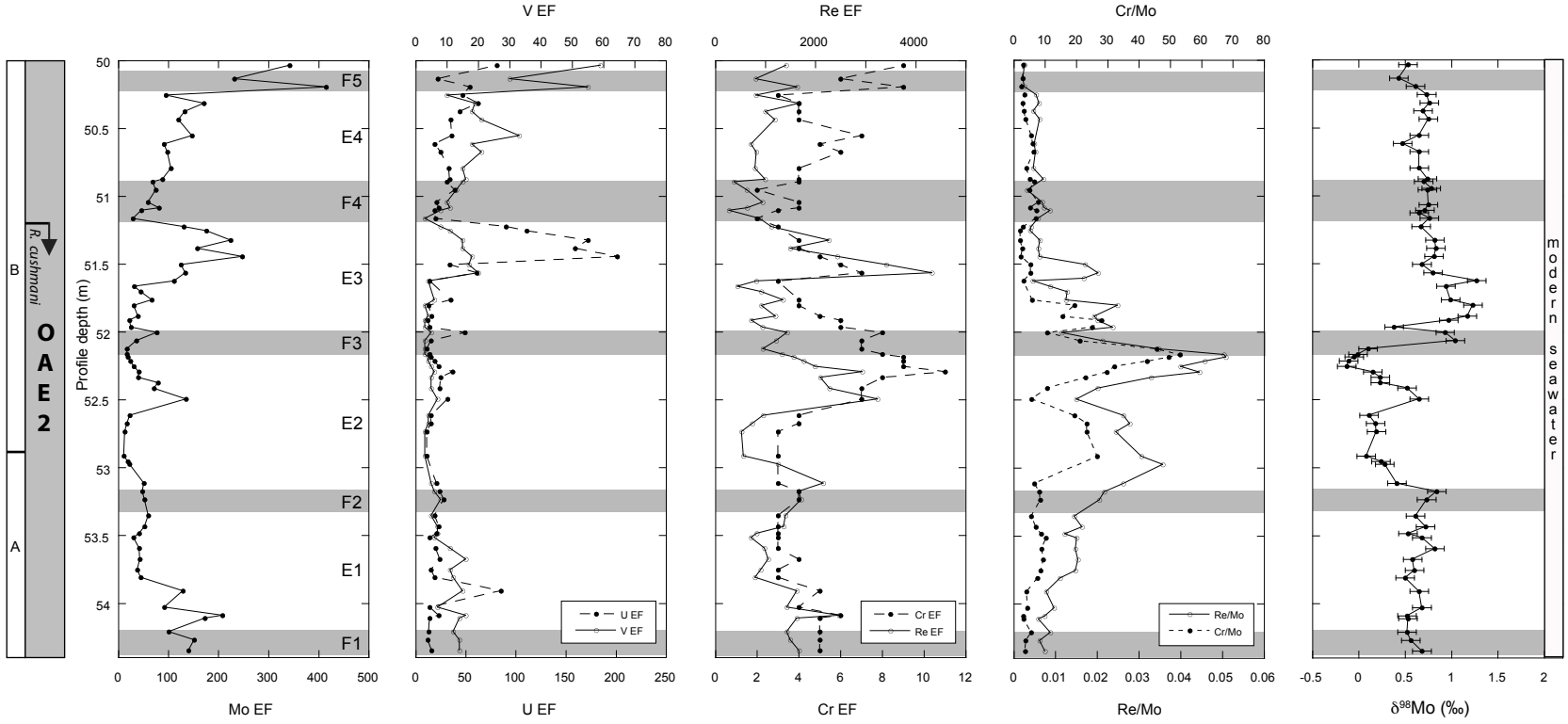

B
A
R. cushmani
OAE 2
Profile depth (m)
F5
E4
F4
E3
F3
E2
F2
E1
F1
Mo EF
V EF
U EF
U EF
V EF
Re EF
Cr EF
Cr EF
Re EF
Cr/Mo
Re/Mo
Re/Mo
Cr/Mo
δ98Mo (‰)
modern seawater

Figure 5

